Effect of ion irradiation on the atomic structure of $Zr_{70}Ni_{30}$ metallic glass: A positron annihilation spectroscopy study

Wafa Boukhemkhem[1,*], Rafik Hazem[2], Mahmoud Izerrouken[3], Matteo Ghidelli[4], Thomas Pardoen[5], Saygin Kuzeci[6], Murat Yavuz Yener[7], Cumali Tav[8] and Ugur Yahsi[8,*]

[1] Laboratory of Research on the Physico-Chemistry of Surfaces and Interfaces (LRPCSI), University of 20 August 1955-Skikda, BP 26, 21000 Skikda, Algeria

[2] Laboratory of Coating, Materials and Environment, University M'Hamed Bougara Boumerdes, 35000, Boumerdes, Algeria

[3] Nuclear Research Center of Draria, BP 43, Sebbala, Draria, Algiers, Algeria

[4] Laboratoire des Sciences des Procédés et des Matériaux (LSPM), CNRS, Université Sorbonne Paris Nord, 93430, Villetaneuse, France

[5] Institute of Mechanics, Materials and Civil Engineering, UCLouvain, Place Sainte-Barbe 2, 1348 Louvain-la-Neuve, Belgium

[6] Physics Department, College of Education for Pure Science, Kirkuk University, Kirkuk 36001, Iraq

[7] BETAM, Fatih Sultan Mehmet Vakıf University Topkapi Campus, Zeytinburnu, Istanbul, Turkiye

[8] Department of Physics, Faculty of Science, Marmara University, 34722 Kadikoy, Istanbul, Turkey

[*]Corresponding authors: w.boukhemkhem@univ-skikda.dz and uyahsi@marmara.edu.tr

Abstract

In this work, doppler broadening spectroscopy (DBS) and positron annihilation lifetime spectroscopy (PALS) measurements were employed to investigate the evolution of irradiation-induced defects in $Zr_{70}Ni_{30}$ binary metallic glass exposed to 93.2 MeV

$^{129}Xe^{23+}$ heavy-ion irradiation at room temperature. The combined results revealed that ion irradiation initially increases the free-volume density with a homogeneous spatial distribution up to a fluence of ($\leq 2\times10^{13}$ Xe cm^{-2}). In contrast, increasing fluence ($> 2\times10^{13}$ Xe cm^{-2}), a reduction in open-volume defects was observed, which could be related to structural relaxation accompanied by modifications in atomic arrangement and defect distribution. Moreover, the correlation between the *S*-parameter and *W*-parameter was discussed to identify the nature of defects affecting the performance of $Zr_{70}Ni_{30}$ metallic glass after ion irradiation.

Keywords: $Zr_{70}Ni_{30}$ binary metallic glass, heavy-ion irradiation, defects, positron annihilation lifetime spectroscopy

1. Introduction

Metallic glasses are considered promising structural candidates for nuclear reactors due to their excellent resistance to irradiation damage. However, the formation and evolution of defects at the atomic level under ion irradiation present an interesting challenge that needs to be studied more thoroughly for their application in harsh operating conditions of nuclear reactors [1, 2]. These environments, characterized by high temperatures varying between 300°C to 700 °C, radiation damage levels reaching up to 100 displacements per atom (dpa), and contact with corrosive compounds, are the main factors influencing the degradation of construction materials, including Zr/ Ni-based alloys, and austenitic stainless steels. The selection of each material is based on its specific properties, which are tailored to particular applications in these environments [3]. Zr-based alloys, in particular, exhibit a very low thermal neutron absorption coefficient (0.008 cm^{-1}), excellent corrosion resistance [4]. Accordingly, they are considered the most prevalent fuel rod cladding material, especially in light-water reactors (LWRs).

With the continuous advancement in nuclear technology, the accident-tolerance of Zr alloy fuel claddings could be improved through several methods proposed in the literature, such as (i) improving the Zr alloy cladding's oxidation resistance by applying appropriate coatings, (ii) using alternative cladding materials that show superior performance compared to Zr alloys, (iii) using the suitable fuel systems that exhibit better thermal conductivity and density [5]. Many researchers have focused on coating layers as thin protective surfaces to improve corrosion or oxidation resistance [6, 7, 8]. Thin film metallic glasses (TFMGs) have emerged as one of the promising coating materials in nuclear structural applications [9]. Specifically, MGs are characterized by a disordered structure and lack of crystalline defects (for example, dislocations and grain boundaries), which usually exist in crystalline materials. This structure is responsible for unique mechanical characteristics, including a high hardness (typically ranging from 5 to 10 GPa), significant yield strength (up to 2 GPa), and relatively high fracture toughness compared to their crystalline counterparts [10, 11]. For example, Wei *et al.* [12] elaborated on the Cu–Zr–Al TFMGs by magnetron sputtering process, reporting good resistance to corrosion and reached higher values for both elastic modulus (145.92 GPa) and hardness (8.18 GPa).

To understand the behavior and performance of these materials in nuclear facilities, different types of particles, such as neutrons [13], electrons [14], and ions [15, 16] have been used in both experimental and simulation studies. Nagase *et al.* [17] found the formation of nano-crystalline phases in $Zr_{66.7}Pd_{33.3}$ and $Zr_{66.7}Cu_{33.3}$ MGs after 2 MeV electron irradiation. On the other hand, despite radiation exposure, the initial amorphous structure was retained in $Zr_{52.5}Cu_{17.9}Ni_{14.6}Al_{10}Ti_5$ and $Zr_{54}Ni_{28}Al_{18}$ MGs irradiated by Ni flux of 3 MeV and 12 MeV, respectively [18, 19]. These contradictory findings can be attributed to the fact that sufficient energy deposited to atoms during irradiation induces

displacements of atoms, leading to high-density fluctuations (a couple of free volumes with anti-free volume) and subsequently improving atomic mobility. The change in atomic structure allows the formation of a new phase incorporated in MGs [20]. Moreover, irradiation has been demonstrated to enhance the corrosion resistance of MGs significantly [21], which mainly offers their possibility to use in industrial field applications, particularly in irradiated environments [8, 22]. For instance, Blink *et al.* [23] proposed the application of Fe-based metallic glass coating in nuclear waste containers to store spent nuclear fuel.

Furthermore, the evolution of the mechanical properties against irradiation lacks sufficient clarity. Previous studies have reported both hardening and softening effects. Chen *et al.* [24] found that at a high radiation dose (1dpa), the precipitate of He bubbles with an average size of 8.23 ± 1.84 nm and the decrease in free volume could be potential factors contributing to the hardening of $Zr_{55}Cu_{30}Al_{10}Ni_5$ MG, as evidenced by an increase in hardness from 5.78 GPa to 6.06 GPa (~ 4.8 % rise). In contrast, Sadeghilaridjani *et al.* [25] found a reduction in mechanical properties due to an enhancement in the amount of free volume without altering the disordered atomic structure. Unlike crystalline materials, MGs exhibit the self-healing process of defects in their microstructure [2]. In other words, the rearrangement of free volume leads to annihilating defects induced by irradiation. More generally, it has been shown that changes in the functional behavior of MGs (e.g., mechanical, chemical, etc.) after irradiation exposure are linked to modifications in their atomic structure, and the variation of free volume, defined as the surplus atomic volume from that the ideal dense, disordered structure [26]. Consequently, understanding defects at the atomic level is key for predicting the performance of MGs in practical applications. However, the study of defects generated by irradiation incidence in MGs is limited in the literature, particularly in binary Zr-Ni systems, with only a few publications discussing

the structure and impact on the performance of these materials [16, 2, 27, 28]. In addition, The Zr-Ni system serves as a simple model binary alloy for studying irradiation effects due to the high glass-forming ability (GFA) with different composition. The specific metallic glass with a composition $Zr_{70}Ni_{30}$ was selected because it lies proximity to the amorphization boundary and exhibits high mechanical properties (hardness and strength), as previously reported [29].

The present research investigates the defects and the evolution of the free volume generated in binary Zr-Ni metallic glass irradiated by swift heavy ions using the positron annihilation spectroscopy (PAS) procedure. PAS is particularly sensitive to microscopic empty spaces and enables high-precision detection of free volume, making it an excellent tool for studying irradiation-induced defects. In this work, we primarily focus on the analysis of the Doppler Broadening Spectroscopy (DBS) depth profile, while the Positron Annihilation Lifetime Spectroscopy (PALS) data serving as supporting information to complement the findings, highlighting the impact of irradiation fluence on the types of defects and their evolution. This investigation extends the previous research [30], which concluded that heavy ion irradiation can induce surface smoothening, leading to enhanced corrosion resistance and modified mechanical properties (initially decreased hardness, followed by an increase at higher fluence).

2. Experimental procedures

2.1. Material and sample preparation

$Zr_{70}Ni_{30}$, TFMGs with an average thickness of approximately 1.2 μm, was deposited onto a monocrystalline Si substrate by magnetron sputtering. The sputtering technique was performed using a suitable target of 99.99 % pure Zr and 99.95 % pure Ni. Further details for the sample preparation can be found in our previous work [31].

2.2. Irradiation experiments

The heavy ion irradiation experiment was performed at room temperature in GANIL (Caen, France) using the IRRSUD experimental line. The metallic glass $Zr_{70}Ni_{30}$ was subjected to 93.2 MeV $^{129}Xe^{23+}$ heavy ions at fluences ranging from 5×10^{12} ions cm^{-2} to 8×10^{13} Xe cm^{-2}. Each part of the five samples was masked with an aluminum sheet, which served as a reference for comparison with the irradiated one. A simulation with SRIM (Stopping and Range of Ions in Matter) code [32] indicates that the Xe ion interaction with $Zr_{70}Ni_{30}$ was dominated mainly by electronic energy losses (S_e), and the energy transfer mainly occurs through inelastic collisions (see **Figure 1**).

2.3. Positron annihilation techniques

The positron annihilation techniques are non-destructive processes used to probe the open structures of solid materials [33], including both crystalline [34] and amorphous systems [35]. In particular, Positron Annihilation Lifetime Spectroscopy (PALS) is a direct way for characterizing free volume. It is often used to measure the open spaces and free volumes within various samples. In this study, PALS measurements were performed using a fast-fast coincidence system, measuring the time interval between two γ-rays: the γ-ray of 1274 keV serving as the start signal and accompanied by positron emission, and the γ-ray of 511 keV, produced by positron annihilation, indicating the stop signal. The positron source was prepared by depositing a solution of about 30 μCi of ^{22}NaCl on a thin aluminum foil (5 μm thick), which was then sandwiched between two sample components. Due to the limited availability of film samples, only one film sample was used per measurement. One side consisted of the film covered, while the other side was the silicon (Si) substrate. Positrons emitted from the source (^{22}Na encapsulated in Kapton) have an energy spectrum ranging from zero up to 546 keV, with an average energy of approximately 182 keV. The low energy positrons around 29 keV, primarily annihilate

within the thin films, while the high energy positrons penetrate through the metallic glass $Zr_{70}Ni_{30}$ and implant into the underlying silicon substrate.

For the γ-ray detection, a plastic scintillator (BC422, Saint-Gobain Crystals, Ohio, USA) coupled to the photomultiplier tubes (PMT R2059, Hamamatsu Photonics Deutschland GmbH, Herrsching, Germany) mounted on a PMT Base (265A, Ortec AMETEK GmbH, Meerbusch, Germany) operating at negative 2010 volts was used. Two constant fractional differential discriminators (CFDD 583B, Ortec AMETEK GmbH, Meerbusch, Germany) were used for the window settings of 1274 keV and 511 keV and for generating timing signals. A time-to-amplitude converter (TAC 266, Ortec AMETEK GmbH, Meerbusch, Germany) was used to convert pulses of different heights into a time-to-pulse-height signal. The converted signals were then fed to a multichannel analyzer (Ethernim MCA 919E, Ortec AMETEK GmbH, Meerbusch, Germany). The spectroscopic data obtained from MCA were analyzed using the LT-92.3 software [36] to determine the lifetime and intensity, thus providing information on the free volume. The system's resolution was about 320 ps, and a million counts were recorded for each run.

In addition, Doppler Broadening Spectroscopy (DBS) has been performed. This positron technique is based on the Doppler broadening of the annihilation gamma, offering valuable insights into the momentum distribution of the annihilated electron-positron couples. When a positron comes into contact with an electron in a material, the momentum of the combined positron-electron system in the annihilation direction is transmitted to the 511 keV gamma line from annihilation, causing it to broaden due to the Doppler shift [37, 38]. The Doppler broadening spectrum can be divided into five distinct parts, focusing on the center and wing parts. Sharpness (*S*) and wing (*W*) parameters are measured by how much the center and wing parts of the peak cover the overall area of the peak [37, 38]. The *S* parameter, which is related to the low momenta of valence

electrons, varies due to positron annihilation in the vacancy defects and within the free volume of the material. Variations in the *S* parameter have been widely reported in the literature as an indicator of changes in free volume within metallic glasses (MGs) [39]. In contrast, the *W* parameter, related to the high momenta of core electrons, varies with the chemical defects.

3. Results and discussion

3.1. Analysis of coincidence Doppler broadening spectroscopy data

Figure 2 presents six profiles of the *S*-parameter as a function of positron incident energy and the corresponding mean depth for both non-irradiated and irradiated $Zr_{70}Ni_{30}$ TFMGs at different fluences. All the profiles are irregular at shallow depths (below 1 keV, corresponding to a mean depth of 5.54 nm) due to the diffusion of positrons and their annihilation near the surface. However, with further increase in depth, all profiles gradually reach a plateau, where the S-parameter converge to stable values. This plateau indicates a homogeneous distribution of defects in the bulk region for all samples. The recorded profiles show a similar trend to those reported for the advanced metallic systems [40]. The data collected within the positron energies above 1 keV will be considered to describe the characteristics of annihilation positron-electron in the samples.

Compared to the non-irradiated sample, the *S* parameter of irradiated films increases with increasing ion fluence up to 2×10^{13} Xe cm^{-2} and beyond displays a slight decrease. The evolution of Doppler characteristics is more evident in **Figure 3**, where the average values of the *S* parameter (<*S*>) are plotted as a function of the Xe ion fluence. It is evident that the <*S*> parameter increases from $0.51 \pm 1.8\times10^{-3}$ in the unirradiated film to almost $0.52 \pm 1.8\times10^{-3}$ in the film irradiated at 2×10^{13} Xe cm^{-2}. The increase of the <*S*> parameter in the first phase can be explained by generating free volumes within the irradiated films.

Similar behavior was observed by Sue *et al.* [41] in Fe-based MGs under 28.8 MeV Ne^{10+} ions irradiation. Subsequently, the *S*-parameter slightly decreases and remains unchanged despite further increasing irradiation fluence to 4×10^{13} Xe cm^{-2} and 8×10^{13} Xe cm^{-2}, indicating a reduction in the amount of free volume. Qiu *et al.* [42] reported that 3 MeV Au^{2+} ion irradiation induced changes in free volume, which affected the mechanical properties of $Ni_{50}Nb_{10}Zr_{15}Ti_{15}Pt_{7.5}Cu_{2.5}$ MG. They demonstrated that the free volume formed at low doses (0.49 and 4.9 dpa) can be annihilated at higher doses (49 dpa), suggesting the formation of regions with local order. Furthermore, another study has demonstrated a good correlation between the increase in defects and displacement damage generated by irradiation [43]. This relationship is particularly pronounced at low fluences, where structural changes in the irradiated thin film are primarily driven by an increase in free volume rather than the modifications in the glassy atomic configuration. However, the accumulation of free volume during cascade collisions reaches a threshold due to saturation effects. As a result, it's possible that the local atomic arrangement relaxes into more stable configurations, thereby reducing the open volume available for positron annihilation. Such changes in defect types can significantly affect the shape parameter, highlighting the interplay between irradiation-induced defects and structural relaxation mechanisms.

As well known, the slope of the *S*-*W* curve serves as a fingerprint to identify the type of defects [44]. Therefore, to define these defects, the surface effect from the samples was removed based on the aforementioned data. Consequently, we plotted the curve of the *S*-parameter versus the *W*-parameter (*S*, *W*), as depicted in **Figure 4 (a)**. The dotted black line represents the linear fit of all data points with a slope towards (-0.54 ± 0.06). The linear correlation between *S*-*W* points signifies the presence of a single type of defect. In the current study, the data points (*S*, *W*) of samples irradiated at 5×10^{12}, 1×10^{13}, and

2×10^{13} Xe cm^{-2} are represented by the colors red, blue, and magenta, respectively. These points gradually shift towards higher values of the *S*-parameter and lower values of the *W*-parameter. They are distributed approximately around the fitted straight line, reflecting that a unique type of defect predominates in these samples. Sue *et al.* [41] observed a similar distribution in the $Fe_{80}Si_7B_{13}$ MG irradiated at 4.6×10^{15} Ne cm^{-2}. As the irradiation fluence increases, the appearance of dispersed points below the fitted line suggests the presence of additional defect types. Hence, the positron annihilation mechanism is not identical. Thus, the process of positron annihilation does not follow the same mechanism.

To clarify this point, we plotted the average values of <*S*> and <*W*>, normalized to the unirradiated reference values S_{uni}, and W_{uni}, respectively, as demonstrated in **Figure 4 (b)**. From this figure, two distinct slopes are clearly observed. The first straight line represents the best correlation - a linear relationship - of the normalized data (S_{nor}, W_{nor}), exhibiting a negative slope at lower fluences ($\leq 2\times10^{13}$ Xe cm^{-2}), indicating the presence of an identical annihilation site where positron trapping occurs. This confirms that a single type of defect is present in each sample. However, at high fluences ($> 2\times10^{13}$ Xe cm^{-2}), the normalized data (S_{nor}, W_{nor}) shift towards the bottom and to the left, with a significant change in slope, revealing the presence of a different type of defect. Flores *et al.* [45] previously demonstrated that shifts in the distribution of the *S*-*W* points indicate that positrons annihilate at different annihilation sites, reflecting structural changes that could be associated with crystallization. In the present case, the specimen exhibits significantly lower <*S*> and <*W*> values, suggesting that positrons predominantly annihilate at different sites. This implies a structural modification that alters the nature of positron interactions, likely due to changes in atomic arrangement and defect distribution. This observation is in accordance with the ion track formation. It is well known that high-energy swift heavy ions (SHIs) induce intense electronic excitations along their ion path,

leading to phenomena such as ion track via electron-phonon interactions. At high fluence, the ion tracks probably accumulate, which is responsible for the material's properties of $Zr_{70}Ni_{30}$ MG. Furthermore, point defects can be generated near the track formed under irradiation, reducing the free volume.

3.2. Positron annihilation lifetime spectroscopy (PALS)

The deconvolution results of the measurement PALS before and after Xe ion irradiation, are summarized in **Table 1**.

The positron lifetime profile of the virgin $Zr_{70}Ni_{30}$ metallic glass consists of three components (τ_1, τ_2 and τ_3), each corresponding to the trapping of positrons in different types of open-volume regions at the atomic scale. The first component (τ_1) is the shortest lifetime, which is attributed to the intrinsic micro-voids, similar to Bernal holes, located between regions of short-range atomic order. This component mostly reflects structural characteristics and includes contributions from para-positronium (p-Ps). For this work, the p-Ps is neglected due to its extremely short lifetime. The second lifetime component (τ_2) represents a combined signal from both the $Zr_{70}Ni_{30}$ thin film and the silicon (Si) substrate. The positron lifetime in defect-free crystalline silicon has been experimentally determined to be approximately 220-230 ps. This range is consistent with theoretical calculations and experimental measurements reported in the literature [46]. However, the τ_2 values obtained in our measurements are significantly higher ranging from 0.247 to 0.272 ns. The value of positron lifetime before irradiation ($\tau_2 = 0.272$ ns) is in good agreement with previous studies for $Zr_{52}Ti_6Al_{10}Cu_{18}Ni_{14}$ MG, which reported a τ_2 value of approximately 0.277 ns [47]. This value is also comparable to those observed in binary $Zr_{60}Ni_{40}$ and $Zr_{50}Ni_{50}$ MGs, where τ_2 values are around 0.24 ns and 0.22 ns, respectively

[48]. This confirms that lifetime τ_2 originate from open-volume within the MG rather than from the Si substrate [46]. The implantation profiles for both the metallic glass and silicon substrate (see supplemental file) demonstrate that while the many positrons penetrate deep into the silicon, a significant fraction are implanted at lower energies (< 30 KeV), within nanometer-scale depths in the film. These near-surface regions are particularly sensitive to defect formation due to the irradiation process. The presence of these defects enhances positron trapping, thereby prolonging the residence time of positrons, and affecting the lifetime spectrum, mainly the lifetime (τ_2) and its intensity (I_2). Since the contribution of the positron lifetime from the Si substrate remains relatively constant, it can be inferred that the observed variation in the lifetime spectrum is primarily attributed to the irradiation-induced modifications in the $Zr_{70}Ni_{30}$ film. Therefore, the second lifetime (τ_2) is interpreted as a reflection of the free volume within the densely packed disorder structure of the MG. The τ_2 value of 0.272 ns, with an associated intensity of 61.3 % for the unirradiated specimen demonstrates the incorporation of significant free volume into the prepared amorphous metallic glass. This is expected, as sputtering is a highly non-equilibrium technique that tends to produce materials with high free volume content. These results are consistent with the findings of Yavari *et al.* [49], who identified excess free volume in metallic glasses. The last component (τ_3), represents the longest lifetime, characterized by lowest intensity, and assigned to the lifetime of ortho-positronium (o-Ps). This appears when positrons are trapped in regions of low electron density, such as voids or holes formed during the preparation process [50]. The observed three component (τ_1, τ_2 and τ_3) for the prepared sample, are in agreement of those reported for other metallic glasses [50, 51]. Similarly, Yang *et al.* [2] reported three comparable lifetime components in a binary metallic glass.

It is clear that the lifetime value (τ_2) is higher than the corresponding values reported in

the literature for the bulk of both Zr and Ni, and it differs from the positron trapping in the monovacancies of the two metals [52]. This suggests the absence of vacancy defects, probably due to the structural relaxation occurring after ion irradiation.

The evolution of the second positron lifetime component (τ_2) and its intensity (I_2) with Xe ion fluence is presented in **Figure 5**. As the ion irradiation fluence increases up to 2×10^{13} Xe cm^{-2}, τ_2 decreases from 0.272 ns to 0.247 ns, corresponding to a relative reduction of approximately 9 %, while I_2 increases from 61.3 % to 75.9 %, (24.8% increment), revealing an inverse relationship between these parameters. The increase in I_2 suggests a higher concentration of free volume defects, as more positrons are trapped within the irradiated thin film. This behavior is attributed to atomic displacements, resulting in loosely atomic packed regions, and the generation of additional free volume. Simultaneously, the decrease in τ_2 reflects a reduction in the average size of these free volumes, which facilitates faster positron annihilation at trapping sites. This trend suggests a redistribution of free volume, leading to a more homogeneous distribution of smaller voids throughout the MG. Before irradiation, positrons in metallic glasses are predominantly trapped in pre-existing shallow open-volume regions [53]. However, high-energy ion irradiation generates new defects that serve as more effective positron traps compared to the original ones. Previous study [2] has reported that vacancy-like defects induced by irradiation in metallic glasses are unstable and tend to transform into extensive free volumes. Similar increase in free volume fraction has been observed both experimentally by Bian *et al.* [54], and in molecular dynamics simulations by Avchaciov *et al.* [55]. Overall, at low fluences ($\leq2\times10^{13}$ Xe cm^{-2}), ion irradiation promotes the homogeneity of smaller free-volume defects distribution in $Zr_{70}Ni_{30}$ MG.

As the ion irradiation fluence increases to 4×10^{13} and 8×10^{13} Xe cm^{-2}, both τ_2 and I_2 tend to reach a saturation level. Although τ_2 shows a slight increase at 4×10^{13} Xe cm^{-2}, it

remains below its initial value, reflecting an overall reduction of ~7%. Meanwhile, the intensity I_2 gradually decreases, probably due to a diminished in the number of open-volume defects. Hori *et al.* [43], reported a significant reduction in free volume in $Zr_{50}Cu_{40}Al_{10}$ metallic glass irradiated by 2.5 and 200 MeV Xe ions at fluences of 1×10^{14} Xe cm^{-2} and 1×10^{13} Xe cm^{-2}, respectively, without making any crystallization. This behavior is mainly attributed to structural relaxation. Similar structural relaxation has been observed in Zr-based MG at high irradiation doses (4 dpa), which resulted in increased hardness from 6.19 to 6.49 GPa [56]. Nagel *et al.* [57] also reported a decrease in free volume during the annealing process of $Zr_{65}Al_{7.5}Ni_{10}Cu_{17.5}$ metallic glass, consistent with our findings. These observations imply that changes in defect concentration, rather than defect size, play a more significant role in determining the material properties and trapping characteristics under heavy ion irradiation. At higher fluences, both parameters remain nearly constant, indicating a saturation point, where further irradiation does not significantly alter the positron trapping characteristics. Notably, in comparison to the DBS results, the intensity I_2 exhibits a trend similar to that of the Doppler broadening *S*-parameter under xenon irradiation conditions (see **Figure 3** and **Figure 5**). This variation in I_2, i.e. defect density, further supports its role as a complementary parameter to *S* following ion irradiation.

Additionally, from the **Table 1**, it is clear that both the third positron lifetime (τ_3) and its intensity (I_3) decrease considerably with increasing irradiation fluence. Specifically, τ_3 decreases from 1.92 ± 0.037 ns for the unirradiated sample to 1.49 ± 0.041 ns, while I_3 drops from 1.90 ± 0.031 % down to 0.768 ± 0.022 %, respectively. This reduction suggests changes in the distribution of the density fluctuation within the disordered structure of the metallic glass, likely affecting both the size and the abundance of voids

or holes. Comparable values were recorded by Vishwanath *et al.* [47] and Flores *et al.* [50]. Moreover, the concentration (I_3) is negligible. Hence, we focus only on τ_2 and I_2 data, which describe the significant characteristics of positron annihilation in $Zr_{70}Ni_{30}$ MG.

The above results demonstrate a strong correlation between the evolution of the intensity (I_2) and the *S*-parameter, supporting the evolution of the mechanicals properties [30]. In particular, structural relaxation occurs through a gradual decrease in free volume size, which can lead to changes in defect distribution. Supplementary research using the transmission electron microscopy (TEM) is required to determine the nature of defects at high-fluence irradiation.

4. Conclusion

In this investigation, the defect evolution of deposited $Zr_{70}Ni_{30}$ thin-film metallic glass after 93.2 MeV xenon heavy ion irradiation at room temperature was studied using advanced positron annihilation spectroscopy technique. At low fluences ($\leq 2\times10^{13}$ Xe cm^{-2}), the *S*-parameter increased initially, and positron annihilation lifetime spectroscopy (PALS) revealed that ion irradiation promotes a more homogeneous distribution of smaller free-volume defects, resulting in changes in the distribution of the short-range order. At higher fluences (up to 2×10^{13} Xe cm^{-2}), the *S* parameter, I_2 and τ_2 values decreased slightly and approached saturation. Moreover, the *S*-*W* analysis indicated a change in the type of defect beyond this fluence, suggesting the formation of defects near the ion tracks. Further investigation is necessary to elucidate the structure of these defects. These results demonstrate that $Zr_{70}Ni_{30}$ metallic glass exhibits excellent resistance to defect accumulation, depending on the level of irradiation fluence.

Acknowledgments

We gratefully acknowledge the GANIL accelerator staff for Xe ion irradiations.

Credit authorship contribution statement

Wafa Boukhemkhem: Conceptualization, Methodology, Formal analysis, Investigation, Writing - original draft, Visualization, Data curation, Writing – review & editing. **Rafik Hazem**: Formal analysis, Methodology, Writing Review & Editing, Validation. **Mahmoud Izerrouken**: Conceptualization, Validation, Project administration, Investigation, Writing - Review & Editing, Visualization, Supervision. **Matteo Ghidelli**: Resources, Review & Editing, Validation. **Thomas Pardoen**: Project administration, Resources, Writing - Review & Editing, Validation. **Saygin Kuzeci:** Investigation, Data curation. **Murat Yavuz Yener:** Investigation, Data curation. **Ugur Yahsi**: Data curation, Resources, Formal analysis, Writing - Review & Editing, Validation.

Data availability statement

All data that support the findings of this study are included within the article.

Conflicts of interest or competing interests

The authors declare no conflict of interest, financial or otherwise.

References

[1] William J Weber, Rodney C Ewing, C Austen Angell, George W Arnold, Alastair N Cormack, Jean Marc Delaye, David L Griscom, Linn W Hobbs, Alexandra Navrotsky, David L Price, et al. Radiation effects in glasses used for immobilization of high-level waste and plutonium disposition. Journal of Materials Research, 12(8):1948–1978, 1997. doi: 10.1557/JMR.1997.0266.

[2] L Yang, HY Li, PW Wang, SY Wu, GQ Guo, B Liao, QL Guo, XQ Fan, P Huang, HB Lou, FM Guo, QS Zeng , T Sun, Y Ren and LY Chen. Structural responses of metallic glasses under neutron irradiation. Scientific reports, 7(1):16739, 2017. doi: 10.1038/s41598-017-17099-2.

[3] Steven J Zinkle and GS Was. Materials challenges in nuclear energy. Acta Materialia, 61(3):735–758, 2013. doi: 10.1016/j.actamat.2012.11.004.

[4] R Krishnan and MK Asundi. Zirconium alloys in nuclear technology. Proceedings of the Indian Academy of Sciences Section C: Engineering Sciences, 4:41–56, 1981. doi: 10.1007/BF02843474.

[5] Steven J Zinkle, Kurt A Terrani, Jess C Gehin, Larry J Ott, and Lance Lewis Snead. Accident tolerant fuels for LWRs: A perspective. Journal of Nuclear Materials, 448(1-3):374–379, 2014. doi: 10.1016/j.jnucmat.2013.12.005.

[6] Chongchong Tang, Michael Stueber, Hans Juergen Seifert, and Martin Steinbrueck. Protective coatings on zirconium-based alloys as accident-tolerant fuel (ATF) claddings. Corrosion reviews, 35(3):141–165, 2017. doi: 10.1515/corrrev-2017-0010.

[7] Egor Kashkarov, Bright Afornu, Dmitrii Sidelev, Maksim Krinitcyn, Veronica Gouws, and Andrey Lider. Recent advances in protective coatings for accident tolerant Zr-based fuel claddings. Coatings, 11(5): 557, 2021. doi: 10.3390/coatings11050557.

[8] Essam Serag, Ben Caers, Paul Schuurmans, Stéphane Lucas, and Emile Haye. Challenges and coating solutions for wear and corrosion inside lead bismuth eutectic: A review. Surface and Coatings Technology, 441: 128542, 2022. doi: 10.1016/j.surfcoat.2022.128542.

[9] WD Luo, B Yang, and GL Chen. Effect of Ar^{+} ion irradiation on the microstructure and properties of Zr–Cu–Fe–Al bulk metallic glass. Scripta Materialia, 64(7):625–628, 2011. doi: 10.1016/j.scriptamat.2010.12.004.

[10] MF Ashby and A Lindsay Greer. Metallic glasses as structural materials. Scripta Materialia, 54(3):321–326, 2006. doi: 10.1016/j.scriptamat.2005.09.051.

[11] Wei Hua Wang. The elastic properties, elastic models and elastic perspectives of metallic glasses. Progress in Materials Science, 57(3): 487–656, 2012. doi: 10.1016/j.pmatsci.2011.07.001.

[12] Xianshun Wei, Chengxi Ying, Jing Wu, Haoran Jiang, Biao Yan, and Jun Shen. Fabrication, corrosion, and mechanical properties of magnetron sputtered Cu–Zr–Al metallic glass thin film. Materials, 12(24):4147, 2019. doi: 10.3390/ma12244147.

[13] Yi-fu Dong, Ming-fei Li, Babafemi Malomo, and Liang Yang. Microstructural evolution in ZrCu metallic glass under neutron irradiation. Computational Materials

Science, 188:110183, 2021. doi: 10.1016/j.commatsci.2020.110183.

[14] T Nagase and Y Umakoshi. Electron irradiation induced crystallization of the amorphous phase in $Zr_{65.0}Al_{7.5}Ni_{10.0}Cu_{17.5}$ metallic glass. Science and Technology of Advanced Materials, 5(1-2):57–67, 2004. doi: 10.1016/j.stam.2003.09.010.

[15] Guoqiang Xie, Lin Shao, Dmitri V Louzguine-Luzgin, and Akihisa Inoue. He ion irradiation induced nanocrystallization in $Cu_{50}Zr_{45}Ti_5$ glassy alloy. Surface and Coatings Technology, 206(5):829–833, 2011. doi: 10.1016/j.surfcoat.2011.04.002.

[16] Naoto Onodera, Akito Ishii, Kouji Ishii, Akihiro Iwase, Yoshihiko Yokoyama, Yuichi Saitoh, Norito Ishikawa, Atsushi Yabuuchi, and Fuminobu Hori. Irradiation effect of swift heavy ion for $Zr_{50}Cu_{40}Al_{10}$ bulk glassy alloy. Nuclear Instruments and Methods in Physics Research Section B: Beam Interactions with Materials and Atoms, 314:122–124, 2013. doi: 10.1016/j.nimb.2013.04.034.

[17] T Nagase, T Hosokawa, and Y Umakoshi. Electron irradiation induced phase transformation in $Zr_{66.7}Cu_{33.3}$ and $Zr_{66.7}Pd_{33.3}$ metallic glass. Scripta materialia, 53(12):1401–1405, 2005. doi: 10.1016/j.scriptamat.2005.08.023.

[18] Alejandro G Perez-Bergquist, Hongbin Bei, Keith J Leonard, Yanwen Zhang, and Steven J Zinkle. Effects of ion irradiation on $Zr_{52.5}Cu_{17.9}Ni_{14.6}Al_{10}Ti_5$ (BAM-11) bulk metallic glass. Intermetallics, 53:62–66, 2014. doi: 10.1016/j.intermet.2014.04.016.

[19] Rachel L Thompson, Yongqiang Wang, and Julia R Greer. Irradiation enhances strength and deformability of nano-architected metallic glass. Advanced Engineering Materials, 20(4):1701055, 2018. doi: 10.1002/adem.201701055.

[20] Michael Myers, EG Fu, Michelle Myers, Haiyan Wang, Guoqiang Xie, X Wang, WK Chu, and Lin Shao. An experimental and modeling study on the role of damage cascade formation in nanocrystalization of ion-irradiated $Ni_{52.5}Nb_{10}Zr_{15}Ti_{15}Pt_{7.5}$ metallic glass. Scripta Materialia, 63(11):1045–1048, 2010. doi: 10.1016/j.scriptamat.2010.07.027.

[21] Zida Zhang, Pengcheng Che, Jian Zhang, Hongbo Fan, Zhiliang Ning, Jianfei Sun, and Yongjiang Huang. Ion irradiation effect on mechanical properties and corrosion resistance of a $Cu_{50}Zr_{50}$ metallic glass. Advanced Engineering Materials, 25(5):2101765, 2023. doi: 10.1002/adem.202101765.

[22] Hongran Zhang, Xianxiu Mei, Yingmin Wang, Zhiguang Wang, and Younian Wang.

Resistance to H^+ induced irradiation damage in metallic glass $Fe_{80}Si_{7.43}B_{12.57}$. Journal of Nuclear Materials, 456:344–350, 2015. doi: 10.1016/j.nimb.2016.03.015.

[23] J Blink, J Farmer, J Choi, and C Saw. Applications in the nuclear industry for thermal spray amorphous metal and ceramic coatings. Metallurgical and Materials Transactions A, 40:1344–1354, 2009. doi: 10.1007/s11661-009-9830-4.

[24] Huaican Chen, Yang Hai, Renduo Liu, Qiantao Lei, Linfeng Ye, Juping Xu, Gang Wang, Wen Yin, Long Yan, and Xingtai Zhou. The microstructure and mechanical properties of He^+ ion irradiated $Zr_{55}Cu_{30}Al_{10}Ni_5$ bulk metallic glass. Intermetallics, 104:52–58, 2019. doi: 10.1016/j.intermet.2018.10.022.

[25] Maryam Sadeghilaridjani, Aditya Ayyagari, Saideep Muskeri, Vahid Hasannaeimi, Jiechao Jiang, and Sundeep Mukherjee. Small-scale mechanical behavior of ion-irradiated bulk metallic glass. Jom, 72: 123–129, 2020. doi: 10.1007/s11837-019-03848-3.

[26] F. Spaepen, Defects in amorphous metals, in: R. Balian, M. Kleman, J. Poirier (editors.), Physics of Defects, North-Hollan Press, Amsterdam, 1981, p. 133-174

[27] Naoto Onodera, Akito Ishii, Yuka Fukumoto, Akihiro Iwase, Yoshihiko Yokoyama, and Fuminobu Hori. Local structure and hardness change of $Zr_{50}Cu_{40}Al_{10}$ bulk glassy alloy after heavy ion irradiation. Nuclear Instruments and Methods in Physics Research Section B: Beam Interactions with Materials and Atoms, 282:1–3, 2012. doi: 10.1016/j.nimb.2011.08.049.

[28] Yifu Wang, Mingfei Li, and Liang Yang. Element dependence of radiation-induced structural changes in metallic glasses. Journal of Non-Crystalline Solids, 533:119933, 2020. doi: 10.1016/j.jnoncrysol.2020.119933.

[29] Matteo Ghidelli, Hosni Idrissi, S´ebastien Gravier, Jean-Jacques Blandin, Jean-Pierre Raskin, Dominique Schryvers, and Thomas Pardoen. Homogeneous flow and size dependent mechanical behavior in highly ductile zr65ni35 metallic glass films. Acta Materialia, 131:246–259, 2017. doi: 10.1016/j.actamat.2017.03.072.

[30] Wafa Boukhemkhem, Mahmoud Izerrouken, Matteo Ghidelli, Thomas Pardoen, Ali Sari, Abdel Yazid Khereddine, and Ali Meftah. Swift heavy ion irradiation effect on structural, morphological and mechanical properties of $Zr_{70}Ni_{30}$ metallic glass. Physica Scripta, 98(8):085311, 2023. doi: 10.1088/1402-4896/ace387.

[31] Matteo Ghidelli, Sébastien Gravier, Jean-Jacques Blandin, Thomas Pardoen, Jean-Pierre Raskin, and Frédéric Mompiou. Compositional-induced structural change in Zr_xNi_{100-x} thin film metallic glasses. Journal of alloys and compounds, 615:S348–S351, 2014. doi: 10.1016/j.jallcom.2013.12.054.

[32] James F Ziegler, Matthias D Ziegler, and Jochen P Biersack. SRIM–the stopping and range of ions in matter (2010). Nuclear Instruments and Methods in Physics Research Section B: Beam interactions with materials and atoms, 268(11-12):1818–1823, 2010. doi: 10.1016/j.nimb.2010.02.091.

[33] Roy Neil West. Positron studies of condensed matter. Advances in Physics, 22(3):263–383, 1973. doi: 10.1080/00018737300101299.

[34] Mahmoud Izerrouken, Rafik Hazem, Ugur Yahsi, Salah Eddine Naceri, Cumali Tav, Saygin Kuzeci, Ali Sari, Fadhela Haid, Ahmad Ishaq, Omar Menchi, and Mostefa Ghamnia. Heavy ion irradiation induced defects in Zircaloy-4. Physica Scripta, 96(4):045008, 2021. doi: 10.1088/1402-4896/abe3bf.

[35] Zsolt Kajcsos, László Marczis, Antal Lovas, Éva Kisdi- Koszó, Dezső Kiss, Csaba Szeles, and Gerhard Brauer. Extensive study of metallic glasses by positron annihilation. Nuclear Instruments and Methods in Physics Research, 199(1-2):327–332, 1982. doi: 10.1016/0167-5087(82)90224-1.

[36] J Kansy. Microcomputer program for analysis of positron annihilation lifetime spectra. Nuclear Instruments and Methods in Physics Research Section A: Accelerators, spectrometers, detectors and associated equipment, 374(2):235–244, 1996. doi: 10.1016/0168-9002(96)00075-7.

[37] Y.C. Jean, P.E. Mallon, and D.M. Schrader. Principles and applications of positron and positronium chemistry. World Scientific, 2003. doi: 10.1142/5086.

[38] A Arrar, M Benhaliliba, A Boukhachem, U Yah¸si, C Tav, A Yumak, and M Amlouk. Optical and photoluminescence spectroscopy analysis and doppler broadening annihilation radiation studies of perovskites based on $La_{1-x}Ni_xMnO_{2.75}$ thin layers. Optik, 224:165678, 2020. doi: 10.1016/j.ijleo.2020.165678.

[39] Katharine M Flores, Biraja P Kanungo, Stephen C Glade, and Palakkal Asoka-Kumar. Characterization of plasticity-induced structural changes in a Zr-based bulk metallic glass using positron annihilation spectroscopy. Journal of non-crystalline solids,

353(11-12):1201–1207, 2007. doi: 10.1016/j.jnoncrysol.2006.11.017.

[40] Abid Hussain, SA Khan, Sandeep K Sharma, Kathi Sudarshan, Saurabh K Sharma, Chetan Singh, and Pawan Kumar Kulriya. Influence of defect dynamics on the nanoindentation hardness in NiCoCrFePd high entropy alloy under high dose Xe^{+3} irradiation. Materials Science and Engineering: A, 863:144523, 2023. doi: 10.1016/j.msea.2022.144523.

[41] Yachao Suo, Lisong Zhang, Tong Guan, Xianxiu Mei, Xiaonan Zhang, Chonghong Zhang, Yitao Yang, Xingzhong Cao, Jianbing Qiang, and Younian Wang. Study on the irradiation damage in Fe-based metallic glasses induced by Ne^{10+} ions. Fusion Engineering and Design, 157: 111635, 2020. doi: 10.1016/j.fusengdes.2020.111635.

[42] YH Qiu, C Xu, EG Fu, PP Wang, JL Du, ZY Hu, XQ Yan, XZ Cao, YG Wang, and L Shao. Mechanisms for the free volume tuning the mechanical properties of metallic glass through ion irradiation. Intermetallics, 101:173–178, 2018. doi: 10.1016/j.intermet.2018.08.006.

[43] F Hori, N Onodera, Y Fukumoto, A Ishii, A Iwase, A Kawasuso, A Yabuuchi, M Maekawa, and Y Yokoyama. A study of defects in electron-and ion-irradiated ZrCuAl bulk glassy alloy using positron annihilation techniques. Journal of Physics: Conference Series, 262(1): 012025, 2011. doi: 10.1088/1742-6596/262/1/012025.

[44] M Clement, JMM De Nijs, P Balk, H Schut, and A Van Veen. Analysis of positron beam data by the combined use of the shape-and wing-parameters. Journal of applied physics, 79(12):9029–9036, 1996. doi: 10.1063/1.362635.

[45] KM Flores, D Suh, RH Dauskardt, P Asoka-Kumar, PA Sterne, and RH Howell. Characterization of free volume in a bulk metallic glass using positron annihilation spectroscopy. Journal of materials research, 17: 1153–1161, 2002. doi: 10.1557/JMR.2002.0171.

[46] Roberto Sennen Brusa, W Deng, GP Karwasz, and Antonio Zecca. Doppler-broadening measurements of positron annihilation with high-momentum electrons in pure elements. Nuclear Instruments and Methods in Physics Research Section B: Beam Interactions with Materials and Atoms, 194(4):519–531, 2002. doi: 10.1016/S0168-583X(02)00953-9.

[47] B Vishwanadh, SK Sharma, PK Pujari, R Kishore, GK Dey, and R Tewari. Influence

of free volume and medium-range order on the deformation response of rapidly solidified and bulk Zr-based ($Zr_{52}Ti_6Al_{10}Cu_{18}Ni_{14}$) metallic glass. Philosophical Magazine, 93(25): 3442–3471, 2013. doi: 10.1080/14786435.2013.810818.

[48] MJ Bernal, RM De la Cruz, R Pareja, and JM Riveiro. Mechanical amorphization

in the Ni-Zr system investigated by positron lifetime spectroscopy. Journal of non-crystalline solids, 180(2-3):164–170, 1995. doi: 10.1016/0022-3093(94)00479-X.

[49] Alain Reza Yavari, Alain Le Moulec, Akihisa Inoue, Nobuyuki Nishiyama, Nicoleta Lupu, Eiichiro Matsubara, Walter José Botta, Gavin Vaughan, Marco Di Michiel, and Åke Kvick. Excess free volume in metallic glasses measured by X-ray diffraction. Acta Materialia, 53(6):1611–1619, 2005. doi: 10.1016/j.actamat.2004.12.011.

[50] KM Flores, E Sherer, A Bharathula, H Chen, and YC Jean. Sub-nanometer open volume regions in a bulk metallic glass investigated by positron annihilation. Acta materialia, 55(10):3403–3411, 2007. doi: 10.1016/j.actamat.2007.01.040.

[51] Yanqing Su, Fuyu Dong, Liangshun Luo, Jingjie Guo, Baoshuai Han, Zhuoxi Li, Baoyi Wang, and Hengzhi Fu. Bulk metallic glass formation: The positive effect of hydrogen. Journal of non-crystalline solids, 358 (18-19):2606–2611, 2012. doi: 10.1016/j.jnoncrysol.2012.06.014

[52] JM Campillo Robles, E Ogando, and F Plazaola. Positron lifetime calculation for the elements of the periodic table. Journal of Physics: Condensed Matter, 19(17):176222, 2007. doi: 10.1088/0953-8984/19/17/176222.

[53] K Sugita, M Matsumoto, M Mizuno, H Araki, and Y Shirai. Electron irradiation damage and the recovery in a Zr-based bulk amorphous alloy $Zr_{55}Cu_{30}Al_{10}Ni_5$. Journal of Physics: Conference Series, 106(1):012024, 2008. doi: 10.1088/1742-6596/106/1/012024.

[54] XL Bian, Gang Wang, HC Chen, Long Yan, JG Wang, Qing Wang, PF Hu, JL Ren, Kang Cheung Chan, N Zheng, et al. Manipulation of free volumes in a metallic glass through Xe-ion irradiation. Acta Materialia, 106:66–77, 2016. doi: 10.1016/j.actamat.2016.01.002.

[55] KA Avchaciov, Y Ritter, Flyura Djurabekova, Kai Nordlund, and K Albe. Effect of ion irradiation on structural properties of $Cu_{64}Zr_{36}$ metallic glass. Nuclear Instruments and Methods in Physics Research Section B: Beam Interactions with Materials and

Atoms, 341:22–26, 2014. doi: 10.1016/j.nimb.2014.06.036.

[56] K Sun, G Wang, YW Wang, HC Chen, L Yan, S Pauly, YH Wu, H Weber, Q Wang, B Huang, et al. Structural rejuvenation and relaxation of a metallic glass induced by ion irradiation. Scripta Materialia, 180:34–39, 2020. doi: 10.1016/j.scriptamat.2020.01.023.

[57] C Nagel, K Rätzke, E Schmidtke, F Faupel, and W Ulfert. Positron-annihilation studies of free-volume changes in the bulk metallic glass $Zr_{65}Al_{7.5}Ni_{10}Cu_{17.5}$ during structural relaxation and at the glass transition. Physical review B, 60(13):9212, 1999. doi: 10.1103/PhysRevB.60.9212.

Figures captions

Figure 11111. Distribution of electronic energy loss (S_e) and nuclear energy loss (S_n) as a function of depth for 93.2 MeV Xe ions in $Zr_{70}Ni_{30}$ metallic glass. The shaded rectangle in the plot indicates the thickness of the analyzed film.

Figure 2. Evolution of *S* parameter versus positron incident energy (keV) as well as the depth (nm) for $Zr_{70}Ni_{30}$ metallic glass before and after Xe ion irradiation at different fluences with the standard deviation. The shaded rectangle in the plot indicates the surface effect.

Figure 3. Variation of the average $\langle S \rangle$ parameter as a function of irradiation fluence for $Zr_{70}Ni_{30}$ metallic glass. The short-dotted lines for guiding the eye.

Figure 4. (a) *S*-*W* curve for unirradiated and irradiated $Zr_{70}Ni_{30}$ metallic glass with the standard deviation. The short-dotted line represents the linear fit of the data points, **(b)** The calculated normalized W_{nor} parameter ($\langle W \rangle / W_{uni}$) versus S_{nor} parameter ($\langle S \rangle / S_{uni}$) for unirradiated and irradiated $Zr_{70}Ni_{30}$ metallic glass. The red line represents the best correlation of the data points (S_{nor}, W_{nor}).

Figure 5. Fluence irradiation dependence of the lifetime component (τ_2) (red triangles) and the corresponding intensity (I_2) (blue triangles) for $Zr_{70}Ni_{30}$ metallic glass with the standard deviation. The short-dotted lines are interconnecting to the data.

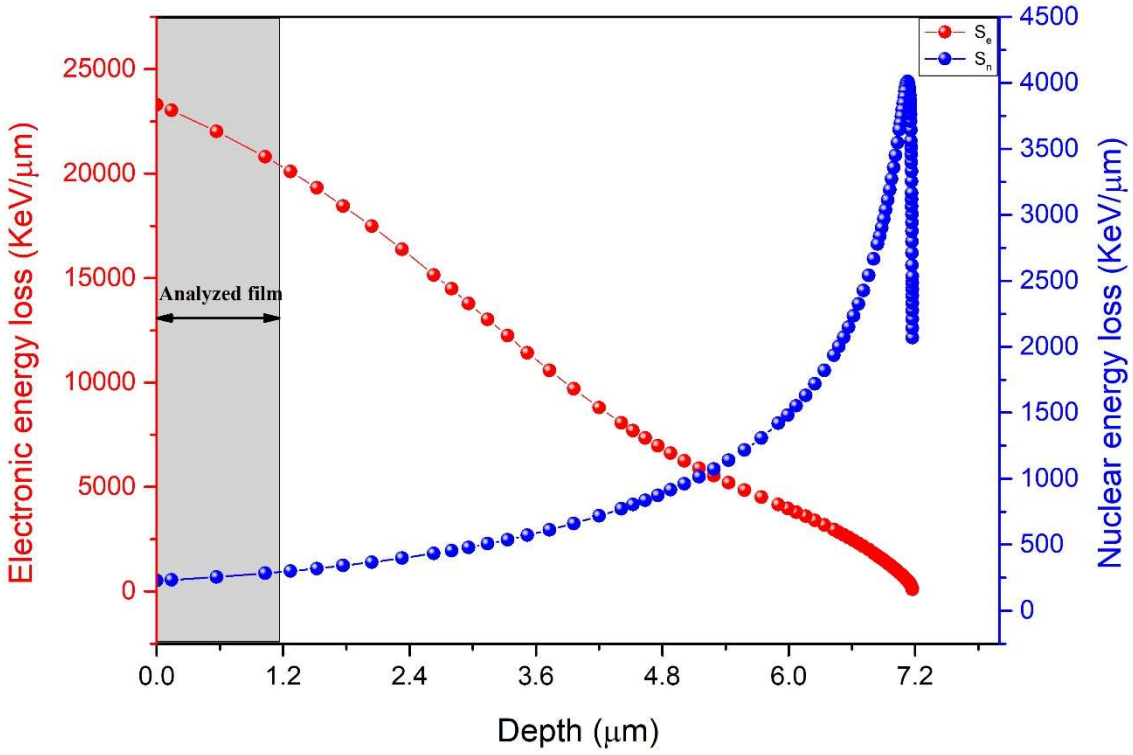


Figure 22221.

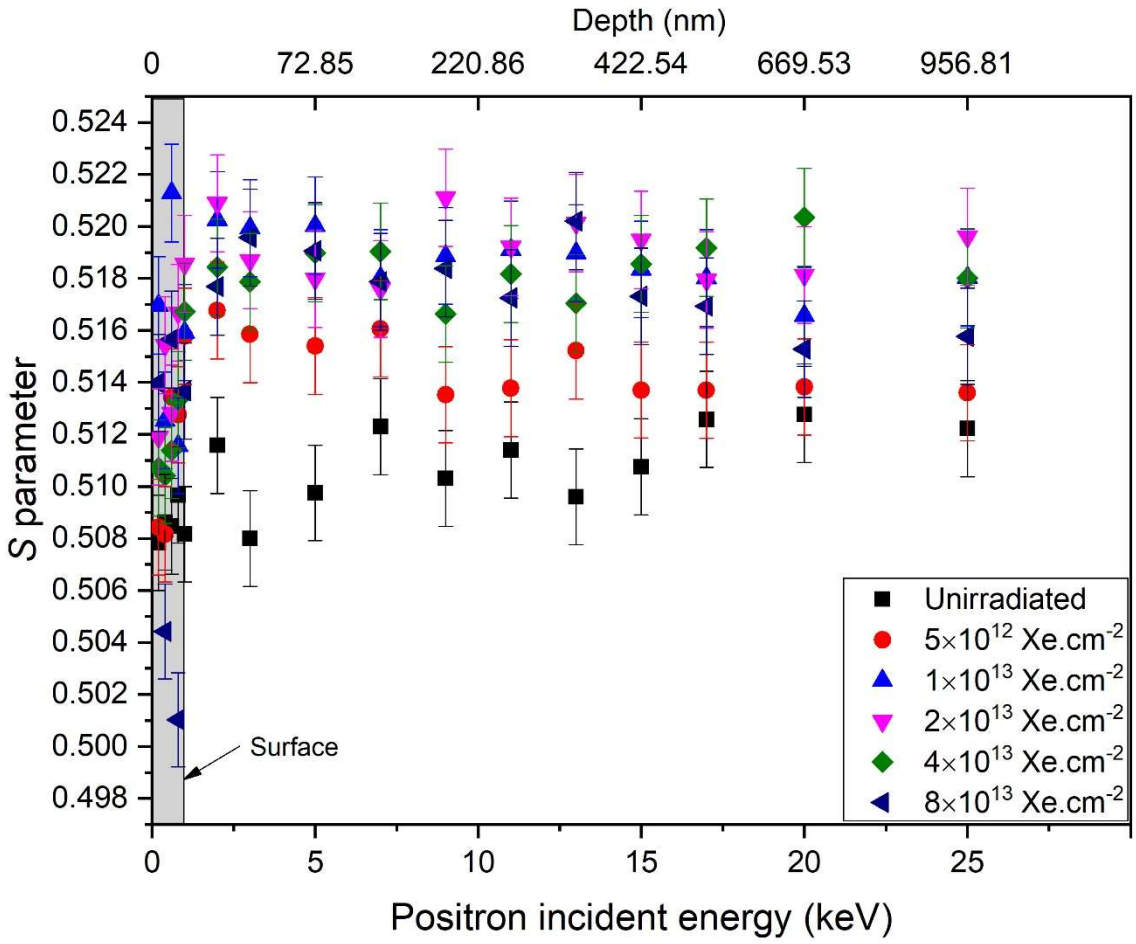

Depth (nm)
0
72.85
220.86
422.54
669.53
956.81
S parameter
0.524
0.522
0.520
0.518
0.516
0.514
0.512
0.510
0.508
0.506
0.504
0.502
0.500
0.498
Surface
Unirradiated
5×10^12 Xe.cm^-2
1×10^13 Xe.cm^-2
2×10^13 Xe.cm^-2
4×10^13 Xe.cm^-2
8×10^13 Xe.cm^-2
0
5
10
15
20
25
Positron incident energy (keV)

Figure 2.

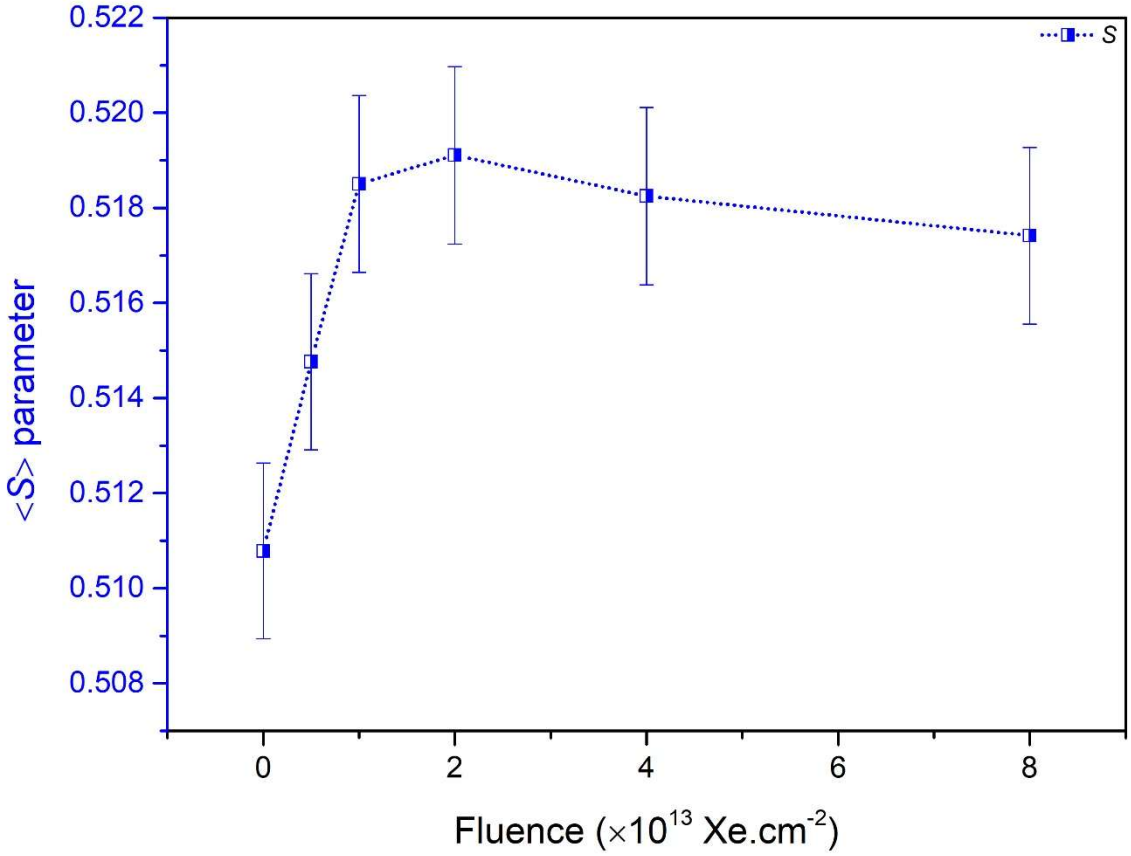

0.522
0.520
0.518
0.516
0.514
0.512
0.510
0.508
<S> parameter
S
0
2
4
6
8
Fluence (×10^13 Xe.cm^-2)

Figure 3.

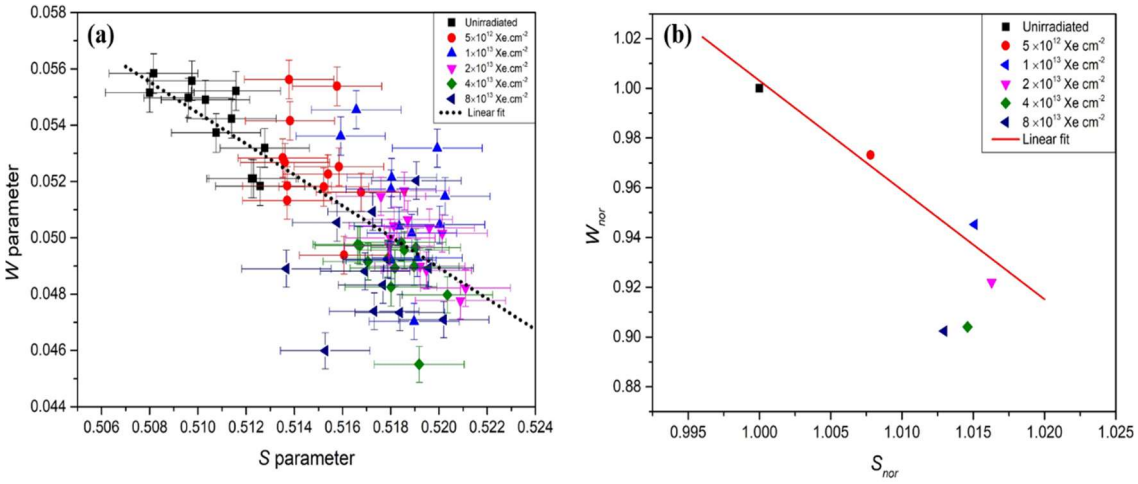

(a)
Unirradiated
5×10^12 Xe.cm^-2
1×10^13 Xe.cm^-2
2×10^13 Xe.cm^-2
4×10^13 Xe.cm^-2
8×10^13 Xe.cm^-2
Linear fit
W parameter
S parameter
0.058
0.056
0.054
0.052
0.050
0.048
0.046
0.044
0.506 0.508 0.510 0.512 0.514 0.516 0.518 0.520 0.522 0.524
(b)
Unirradiated
5 ×10^12 Xe cm^-2
1 ×10^13 Xe cm^-2
2 ×10^13 Xe cm^-2
4 ×10^13 Xe cm^-2
8 ×10^13 Xe cm^-2
Linear fit
W_nor
S_nor
1.02
1.00
0.98
0.96
0.94
0.92
0.90
0.88
0.995 1.000 1.005 1.010 1.015 1.020 1.025

Figure 4.

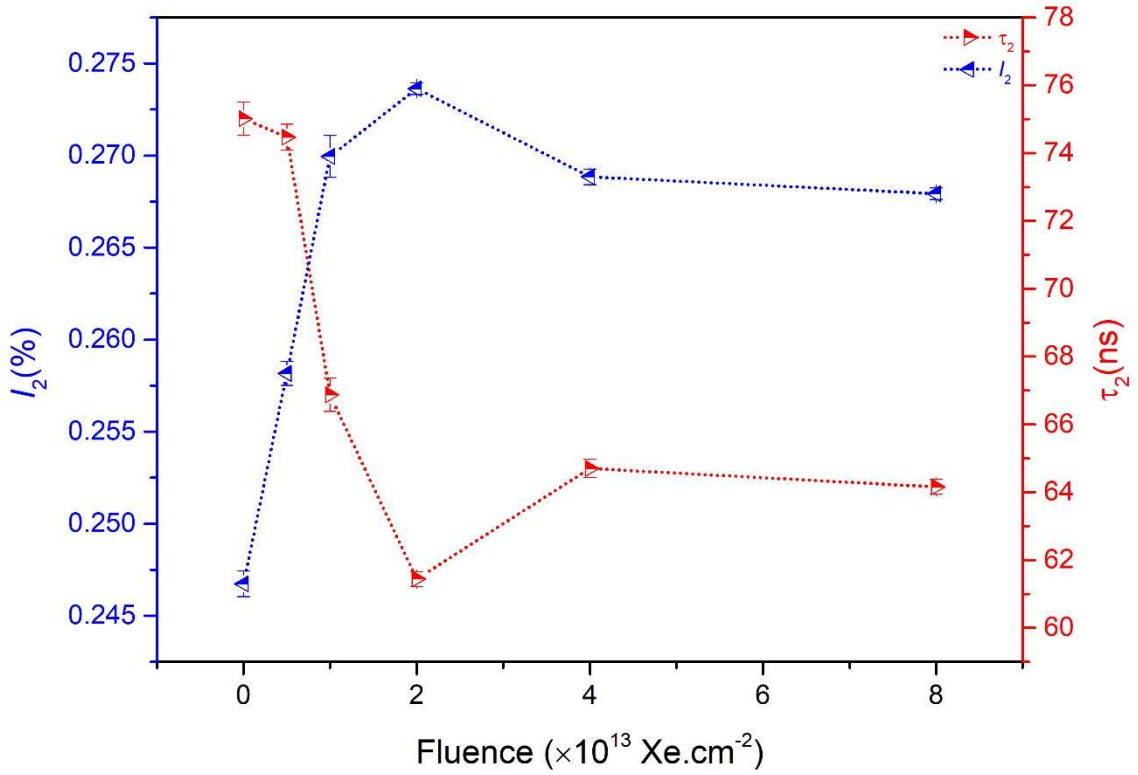

0.275
0.270
0.265
0.260
0.255
0.250
0.245
I_2(%)
78
76
74
72
70
68
66
64
62
60
τ_2(ns)
τ_2
I_2
0
2
4
6
8
Fluence (×10^{13} Xe.cm^{-2})

Figure 5.

Tables

Table 1. Positron annihilation lifetimes components (τ_1 ,τ_2 and τ_3) with their corresponding intensities (I_1, I_2 and I_3) for the virgin and irradiated $Zr_{70}Ni_{30}$ metallic glass at different fluences.

Table 1.

Irradiation fluence (Xe cm^{-2})	τ_1(ns) I_1 (%)	τ_2 (ns) I_2 (%)	τ_3 (ns) I_3 (%)
0	0.150±0.001 (36.8±0.390)	0.272±0.0009 (61.3±0.380)	1.92±0.037 (1.90±0.0310)
5×10^{12}	0.148±0.002 (31.1±0.350)	0.271±0.0007 (67.5±0.350)	1.93±0.048 (1.45±0.0310)
1×10^{13}	0.148±0.002 (25.5±0.620)	0.257±0.0009 (73.9±0.620)	1.70±0.076 (0.690±0.0320)
2×10^{13}	0.151±0.002 (23.9±0.170)	0.247±0.0004 (75.9±0.170)	1.77±0.049 (0.588±0.0220)
4×10^{13}	0.151±0.001 (26.1±0.230)	0.253±0.0005 (73.3±0.230)	1.66±0.053 (0.680±0.0220)
8×10^{13}	0.154±0.001 (26.4±0.170)	0.252±0.0004 (72.8±0.170)	1.49±0.041 (0.768±0.0220)